Acoustic parametric instability, its suppression and a beating instability in a mesoscale combustion tube

Ajit Kumar Dubey[1,2,3], Yoichiro Koyama[1], Nozomu Hashimoto[1], and Osamu Fujita[1].

[1]Division of Mechanical and Space Engineering, Hokkaido University, Kita 13 Nishi 8 Kita-ku, Sapporo, Hokkaido, 060-8628, Japan

[2]Institute of Fluid Science, Tohoku University, 2-1-1 Katahira, Aoba-Ku, Sendai, Miyagi, 980-8577, Japan

[3]Research Alliance Center of Mathematical Sciences, Tohoku University, 6-3 Aoba, Aramaki, Aoba-Ku, Sendai, Miyagi, 980-8578, Japan

Corresponding author: Osamu Fujita
Division of Mechanical and Space Engineering, Hokkaido University, Kita 13 Nishi 8 Kita-ku, Sapporo, Hokkaido, 060-8628, Japan

TEL: +81-11-706-6385
FAX: +81-11-706-7841
E-mail: ofujita@eng.hokudai.ac.jp

Abstract

The present work reports thermo-acoustic instability in a mesoscale tube of diameter 8 mm (> quenching diameter) and length 702 mm. Mixtures with Lewis number, *Le*~ 0.8 (rich $C_2H_4/O_2/CO_2$), 1.05 (lean $C_2H_4/O_2/CO_2$) and 1.34 (lean $C_2H_4/O_2/N_2$) are used. Several new flame responses are observed. For lower burning velocity mixtures, flame extinction is observed due to heat loss when primary instability transforms to secondary instability for all *Le* mixtures. However, parametric cellular structures which are characteristic of parametric instability are observed only for *Le* of 0.8. It is proposed based on calculations and experiments that parametric structures will be observed only when diameter of tube is two times larger than the characteristic wavelength of parametric instability. If the tube diameter doesn't allow formation of parametric structure whirling and counter-rotating flames are observed instead of parametric structures. Suppression of acoustic parametric instability is observed for higher burning velocity mixtures with *Le*>1 and its mechanism is discussed. For a range of $S_{L,}$ a beating instability is observed for CO_2 diluted mixtures of *Le*>1, where pressure oscillation and flame motion show beating oscillations of frequency around 15 Hz. This beating instability is believed to be caused by non-linear interaction of acoustic instability with pulsating instability of flame front which is caused due to combined radiative and convective heat loss. Due to CO_2 dilution, the radiative heat losses could play a significant role in inducing pulsating instability.

Keywords: Mesoscale combustion, Pulsating instability, Combustion tube, Beating instability, Parametric instability

1. **Introduction**

Flame propagation in tube is a fundamental topic in combustion science and has been studied for a long time. Flames propagating in a tube from open to closed end are known to generate thermoacoustic instabilities (sustained pressure oscillations)[1] [2] as well as flame front instabilities (flame oscillation and corrugated flame-front formation) [3] due to interaction between flame and acoustic modes of tube. Two forms of thermoacoustic instability are observed in such experiments depending on laminar burning velocity, S_L of mixture; a primary acoustic instability[4] with lower growth rate and a secondary instability [5] with comparatively higher growth rate. In a systematic experiment by continuously increasing S_L, different regimes (I to VII) can be identified depending on flame shape transformations and growth of pressure fluctuations. Flame and pressure history for these regimes are outlined in Fig. 1 and are briefly described here. Regime I: curved flame propagates without any pressure oscillation. Regime II: curved flame starts vibrating and pressure fluctuations are observed of primary acoustic instability. Regime III: vibrating curved flame turns to vibrating flat flame and primary acoustic instability is saturated. Regime IV: corrugations are developed on vibrating curved leading to turbulent flame and primary instability is followed by secondary instability. The corrugations on flame front are due to a parametric instability. Regime V: vibrating curved flame transform directly to turbulent flame through parametric instability. The minimum S_L to observe regime V is called critical and is studied in detail in our previous work. Until regime V, pressure fluctuations of only fundamental mode are observed. Secondary instability of higher acoustic modes are generated if the S_L is further increased [5][4]. Regime VI: first harmonic instability transforms to fundamental mode as the flame propagates downwards. Parametric structures corresponding to both harmonics of the tube are observed. Regime VII show instability first three modes of the tube.

Pressure[7] [8][9] and velocity coupling [10] mechanism were studied as possible mechanisms for occurrence of acoustic instability in propagating flames. Velocity coupling mechanism(flame area variations cause heat release fluctuations) predicted higher growth rates consistent with propagating

flame experiments[4] and correctly explained the effect of geometrical parameters[11]. Laser irradiation technique which can artificially modify flame shape and area has been applied to study onset of primary[12] and parametric instability[13][14] in downward propagating flames and also understand turbulization mechanism of flat flame[15][16]. Effect of Lewis number (*Le*) on primary[17] and secondary instability[5][14][6]had also been investigated. Thermoacoustic instabilities were also studied in annular space of width 11 mm[18] and Hele-Shaw cells of width in the range 4 mm to 10 mm[19] to understand the effect of Markstein number. Secondary instability had also been found numerically in upward propagating flames for a certain range of frequencies if acoustic forcing reaches a critical amplitude [20].

The secondary instability during downward propagating flame experiment originates due to parametric instability of flame front propagating in acoustic field. During this instability, corrugated structures of a certain wavelength are generated on the flame front when acoustic fluctuations reach a critical amplitude. If the tube diameter is near this critical wavelength, then the acoustic parametric instability nears its limit length scale and interesting phenomenon can be anticipated. Heat loss from flame to walls can also have a role at such scales. Thermoacoustic instability has been mostly studied in experimental systems where heat loss doesn't affect acoustic or flame instabilities. However, thermoacoustic instability at scale where heat loss from propagating flames can become important is not often studied. Study of such instability can also be of practical significance as it will improve understanding of flame instabilities possible in miniature combustion devices which has seen rapid developments in recent decades[21][22] due to need of small scale and portable power generators. Due to small scale, the effects of heat losses are very important, and a variety of flame instabilities are observed in micro and mesoscale combustion [21].Recently, interesting flame shape transitions due to heat loss and subsequent propagation in narrow gap Hele-Shaw cells has been reported for very lean hydrogen/air mixtures [23].

It is known that at small scales, heat losses can cause flame extinction. Moreover, heat losses can also modify the stability limits of flat flames and close to extinction a pulsating instability due to heat loss

had also been predicted [24]. Necessarily, this pulsating instability is a high Lewis number, *Le* phenomena which has been reported for lean *n*-butane/oxygen/helium ($Le \approx 4.0$) flames near lean flammability limit [25]. Presence of heat losses can reduce the critical *Le* for observation of pulsating instability and has also been reported for $Le \approx 1.9$ flames of lean propane/air mixtures[25][26]. Recently, thermoacoustic instability has been reported in flames propagating in small space between plates, called Hele-Shaw cells and it was found that for very narrow spacing, thermoacoustic instability could not be generated[19] but for spacing around 8-10 mm parametric instability can be generated. For the occurrence of parametric instability, the ratio of dimensions and critical wavelength of parametric instability is an important parameter as is discussed in detail in our results. However, such study in narrow tubes where flame doesn't have space in normal direction to generate parametric instability has not been reported yet. Recently, we have tried to clarify the effects of diameter on various aspects of thermoacoustic instability and observed a critical diameter where range of mixture conditions where parametric instability can be observed is maximized [27]. Just below this critical diameter, experiments show that secondary instability is suppressed at higher S_L conditions. Understanding this phenomenon is the motivation behind this work which is depicted in Fig. 2.

With the aim of studying thermoacoustic instability in mesoscale combustion, this work presents study on downward flame propagation in a tube of inner diameter 8 mm which is above the usual quenching diameter for mixtures applied in this work. Various new thermoacoustic instability regimes observed in experiments are discussed along with their possible mechanisms.

2. Experimental method

The schematic of experimental setup is shown in Fig. 3 and is similar to the setup reported in our earlier works [11][5] [27]. The setup consists of a transparent acrylic tube of inner diameter 8.0 mm and length 702.0 mm which is fixed vertically. The tube was closed at bottom and a lid was fixed on springs on the upper side which can be opened by the action of an electromagnet.

Lean $C_2H_4/O_2/CO_2$ mixtures of equivalence ratio 0.8 for which Lewis number, *Le* based on deficient reactant was 1.05 were used as combustible test mixtures Experiments were also performed with rich $C_2H_4/O_2/CO_2$ mixtures of equivalence ratio 1.2 (Le~0.8) and lean $C_2H_4/O_2/N_2$ mixtures of equivalence ratio 0.8 (Le~1.34) to study the effect of *Le*. CO_2 /N_2 dilution was varied to change laminar burning velocity of a freely propagating adiabatic premixed flame (S_L) of the mixtures. The properties of these mixtures are tabulated in Table 1 (Le~1.05), Table 2 (Le~0.8) and Table 3 (Le~1.34). Same mixtures have also been used in our earlier works[5] [6] and one could refer to [6] for more information on their properties.

In an experiment, a mixture was filled in the combustion tube at atmospheric pressure and allowed to become quiescent for four minutes, then upper lid was opened by action of an electromagnet and simultaneously the mixture was ignited using a spark near the open end. Hence, the tube had one end open and another end closed during the flame propagation. The flame propagation is recorded using a high-speed camera FASTCAM at 1000 or 2000 frames per second. The resolution of flame images is lower than because the tube diameter is 87.75 times lower than the length and a single camera is used to capture the total length. This is done to relate the flame propagation history to the pressure history. The pressure fluctuations are also simultaneously measured at 10 kHz using a dynamic pressure sensor PCB Piezotronics 106B52 at the bottom of the tube.

Table 1. Mixture composition and properties for lean $C_2H_4/O_2/CO_2$ mixtures of equivalence ratio 0.8 (Le~1.05)

C_2H_4 (%)	**O_2 (%)**	**CO_2 (%)**	**S_L (cm/s)**	**T_b** (K)	**δ (cm)**	**Le**	**Regime**
5.45	20.43	74.12	**10.04**	1717	0.012863	1.045	I

5.75	21.56	72.70	**12.51**	1787	0.010394	1.048	III
6.02	22.58	71.40	**15.00**	1850	0.008723	1.05	IV-N
6.28	23.56	70.16	**17.51**	1907	0.007516	1.052	IV-N
6.52	24.44	69.04	**20.00**	1957	0.006617	1.054	IV/IV-N
6.74	25.28	67.98	**22.50**	2002	0.005914	1.056	IV
6.95	26.07	66.98	**25.00**	2042	0.005348	1.057	Beating
7.16	26.84	66.00	**27.54**	2081	0.004878	1.059	Beating
7.35	27.56	65.08	**30.00**	2115	0.004498	1.061	Beating
7.53	28.25	64.21	**32.50**	2146	0.004169	1.062	Beating
7.71	28.92	63.37	**34.98**	2174	0.003889	1.063	VI-beating
7.88	29.56	62.56	**37.50**	2201	0.003646	1.065	VI-beating
8.06	30.21	61.74	**40.01**	2225	0.003432	1.066	VI-beating
8.21	30.80	60.99	**42.50**	2247	0.003242	1.067	VI-N
8.38	31.41	60.21	**45.00**	2269	0.003073	1.069	N-N

Table 2. Mixture composition and properties for rich $C_2H_4/O_2/CO_2$ mixtures of equivalence ratio 1.2 (Le~0.8)

C_2H_4 **(%)**	O_2 **(%)**	CO_2 **(%)**	S_L (cm/s)	T_b (K)	$\boldsymbol{\delta}$ **(cm)**	*Le*	Regime
7.619	19.05	73.33	**11.00**	1858	0.011779	0.79	IV-N
9.42	23.55	67.03	**25.00**	2128	0.005262	0.80	VI

Table 3. Mixture composition and properties for lean $C_2H_4/O_2/N_2$ mixtures of equivalence ratio 0.8 (Le~1.34)

C_2H_4 **(%)**	O_2 **(%)**	N_2 **(%)**	S_L (cm/s)	T_b (K)	$\boldsymbol{\delta}$ **(cm)**	*Le*	Regime
4.16	15.61	80.22	**24.99**	1869	0.008552	1.343	IV-N
4.64	17.41	77.94	**35.02**	2012	0.00608	1.338	IV
4.87	18.26	76.87	**40.00**	2075	0.005313	1.336	N-N

3. Results and discussion

Flame regimes observed for $C_2H_4/O_2/CO_2$ mixtures with Le≈1.05 is discussed in sections 3.1, 3.2 and 3.3. Then, results with *Le*≈0.8 and 1.34 are discussed in section 3.4 to explain the effect of *Le* and dilution gas.

3.1. Flame regimes at $S_L \leq 20$cm/s

The flame response observed in current 8 mm diameter tube are different from the responses observed in wider tubes e.g. tubes with inner diameter 30 mm or larger[2][11][5] due to influences of geometry along with heat and acoustic losses. To discuss the flame responses observed in current work, the regime numbers, I-IV are assigned in a manner consistent with our earlier works[5][11] and one should refer to these for more details on flame behavior during these regimes. Here, we only briefly describe the flame responses which are common with our earlier experiments and more emphasis is placed on responses unique to narrow tubes. The flame propagation videos of various new regimes are presented in the supplementary file.

For S_L of 10 cm/s, a curved flame propagates without any acoustic instability (regime I). For S_L of 12.5 cm/s, a curved flame propagates with acoustic instability and the curved flame transitions to a flat flame which oscillates at fundamental frequency (regime III). Pressure fluctuation during this regime is shown in Fig. 4 (a). This rise of pressure fluctuation amplitude is due to primary acoustic instability. Pressure oscillation rises in two stages as shown in Fig. 4 (a); in the first stage pressure rises with higher growth rate and flat flame is formed from curved flame; in second stage pressure rises at slightly lower growth rate when the flat flame propagates downwards. To understand this difference in growth rates, we recall the two mechanisms for growth rate of primary acoustic instability which occurs due to positive coupling between heat release from flame and the pressure fluctuations. First, velocity coupling where the heat release rate is modulated by flame area perturbations. Second, pressure coupling where the heat release is modulated by flame speed perturbations due to adiabatic temperature fluctuations. Pressure coupling is known to be much weaker than the velocity coupling [4]. The first

stage growth rate is higher because flame area changes as the curved flame changes to flat flame and the mechanism of acoustic growth is velocity coupling [10]. Whereas, in the second stage flame area remains mostly constant because a flat flame propagates so velocity coupling cannot act and the mechanism for growth is the pressure coupling [7].

For S_L of 15 and 17.5 cm/s, a flame instability regime specific to the narrow tubes is observed termed as regime IV-N where N stands for narrow. During regime IV-N, curved flame turns to vibrating flat flame due to action of pressure fluctuations. Pressure fluctuations which are in phase with flame oscillations are shown in Fig. 4 (b) for this regime. The change from a curved flame near ignition to a near planar flame as the flame propagates down is shown in Fig. 5 (a). The vibration of flame can be clearly seen in the supplementary file which shows movie of regime IV-N. Thereafter, flame attempts to generate the acoustic parametric instability of flame but corrugated structures which are characteristics of parametric instability are not observed. A sudden increase in acoustic pressure is observed which correlates with increase in flame surface area around 2 s as shown in Fig. 5 (b). After one cycle of oscillation, flame surface area reaches a maximum at 2.119 s after which flame area reduces and extinction happens. Figure 5 (b) shows the flame images prior to extinction. This extinction can be due to effect of heat loss and stretch. So, even if the effect of heat loss permits steady propagation of a vibrating planar flame at lower S_L, vibrating flame structure with higher flame area as shown in Fig. 5 (b) is more affected by heat loss and is extinguished. The acoustic velocity also stretches the flame which can be a factor in the extinction. The pressure trace for this regime, Fig. 4 (b) also shows sudden decrease after a few acoustic oscillations of higher amplitude because the flame extinguishes. Similar, flame extinction at the onset conditions of parametric instability were also observed for Le = 0.8 ($C_2H_4/O_2/CO_2$) and Le =1.34 ($C_2H_4/O_2/N_2$) mixtures. Their results are discussed in section 3.4.

On further increasing S_L to 20 and 22.5 cm/s, regime IV is observed where curved flame at ignition turns to flat flame (Fig. 6 a), then parametric instability of flame front happens, and rapidly fluctuating

flame (Fig. 6 (b) and (d)) can propagate until the closed end in some cases and extinguishes sometime before reaching the closed end in some cases. However, owing to smaller tube diameter and thus lower Reynolds number it is difficult to say that this rapidly fluctuating flame is "turbulent" even when the flame propagation speed due to secondary instability is as high as five times the laminar burning velocity of mixtures. Fluctuations in flame luminosity and position can also be clearly seen in Fig. 6 (b)). The pressure trace for this regime (Fig. 4(c)) shows that the peak pressure fluctuation amplitude is larger than 4 kPa which is much higher than the peak pressures of primary acoustic instability indicates that it certainly is the stronger secondary instability which happens due to parametric instability of the flame front. However, the form of acoustic parametric instability in narrow tubes is different compared with that in larger diameter tubes where corrugations of characteristic wavenumber appear on the flame front which transform to fluctuating turbulent flames generating larger pressure fluctuation amplitudes. This can be clearly observed from flame images shown in Fig. 6 where corrugated structures (as shown in Fig. 1) are not observed on the flame front.

The acoustic parametric instability is generated when acoustic fluctuation amplitude reaches a certain value, then, corrugations of a specific wavenumber are generated on the flame front[3]. The wavenumber and acoustic fluctuation amplitude at the onset of parametric instability can be determined by stability analysis of planar flame subjected to acoustic perturbation and are found to depend on mixture properties and acoustic frequency. We have presented such calculations in section 3.5. Based on the calculation, the characteristic wavelength of structures for mixture with S_L=20 cm/s is found to be 4.9 mm. The diameter of the current tube, 8 mm is very close to this characteristic wavelength at the onset of parametric instability. Effect of wall, boundary layer, heat loss and acoustic loss may also limit the formation of corrugated structures at its characteristic wavenumber in the present tube. (Relevant heat and acoustic loss analysis are discussed in section 3.3.) Hence a corrugated structure is not clearly observed at onset of parametric instability. A criterion to observe the parametric structures has been discussed in detail in section 3.5. The fluctuating flame sometime shows a whirling

like motion as in Fig. 6 (c). Some other peculiar flame front structures are shown in Fig. 6 (e). It appears as if sometime structures tend to form on the flame front when it is not perpendicular to the direction of overall motion as 6 (e). At some instances the flame separates into various packets and coalesces later. These new observations regarding acoustic parametric instability are due to the nearness of tube diameter to the characteristic wavelength. Moreover, corresponding experiments in Hele-Shaw cell[19] and annular gap[18] didn't show such modes at a channel or gap width of 8 mm because structures can always form on the flame front due to available space in a direction normal to the flame propagation as discussed in section 3.5.

3.2 Beating instability with suppression of parametric instability

On further increasing S_L in wider tubes, regime V (transition to parametric instability directly from vibrating curved flame without transition to flat flame) and VI and VII showing higher harmonic parametric instability are observed[5]. Interestingly, in current experiments no such regimes are observed. Instead, a new regime is observed at S_L of 27.5 cm/s termed beating. Analysis of pressure fluctuations clearly show presence of two dominant frequencies corresponding to fundamental and first harmonic modes of the tube. The pressure fluctuations decomposed in two range of frequencies are shown in Fig. 7. The flame images at various instances are shown in Fig. 8. Figure 9 shows the flame front history as the flame propagates from open to closed end. It can be clearly seen that the flame vibrates at two different frequencies (Fig. 9). In the upper part of tube, primary instability of first harmonic i.e. a flat flame vibrating at first harmonic frequency of the tube is observed (Fig. 8 (a) and Fig. 9). Interestingly, primary instability of first harmonic is never observed in wider tubes due to lower acoustic losses and the first harmonic instability is observed only in the form of parametric instability with maximum amplitudes larger than 5 kPa as pressure fluctuations are high enough to swiftly cause parametric instability of higher modes[5].

The flame oscillates between a curved and flat front as shown in Fig. 8 (b). Such beating instability has never been reported for propagating flames in tubes. Parametric instability is completely suppressed during this phenomenon.

To elucidate further, pressure, flame position and luminosity fluctuations for around two beating cycles are shown in Fig. 10. The flame luminosity is calculated for a flame image by changing the flame to gray scale and summing over the intensities over the pixels. The fluctuation of flame position is calculated along a mean position when flame also moves downward at a constant speed. From Fig. 9 it can be seen that flame moves at an almost constant speed when it vibrates at fundamental frequency which was found to be 25.22 cm/s which is slightly lower than the S_L of this mixture 27.5 cm/s (possibly due to heat loss or wall effect). The flame motion and pressure oscillation show completely in-phase beating behavior i.e. when flame is at its farthest location pressure is also maximum. It was confirmed that there is only amplitude modulation no frequency modulation because frequency only varies slightly. It can also be observed that the amplitude modulation is not complete and minimum amplitude is only 50 % of the maximum amplitude. The luminosity fluctuations which can also qualitatively represent the heat release fluctuations are slightly out of phase to the pressure oscillations but can still cause sustained pressure oscillations by satisfying Rayleigh criterion.

Beating occurs usually when waves of two frequencies close to each other interfere. In that case the frequency of the beat is equal to the difference of the two frequencies. So, we looked into the dominant frequencies near the fundamental mode. The dominant frequencies are shown in Fig. 11. It can be seen that the two dominant frequencies are 98.7 and 91.2 Hz. If the beating is due to the interference of these two frequencies then the beat frequency should be around 7.5 Hz. The beating frequency was measured from the pressure signal for various S_L and is shown in Fig. 12. It can be seen that it is in the range 15-25 Hz and increases with increasing S_L. For S_L=27.5 cm/s the beating frequency is 15 Hz

which is higher than the expected 7.5 Hz. Hence it is possible that the mechanism of this beating instability is different than just the interference of two frequencies. This beating instability is clearly observed until S_L of 40.0 cm/s. In the last section of this manuscript we present our hypothesis for existence of this beating instability.

3.3 Flame response at higher S_L: Emergence and suppression of parametric instability of first harmonic

On increasing the S_L to 35.0 cm/s, another new flame response is observed termed as VI-beating. (Regime VI in wider tubes secondary instability of first harmonic is followed by secondary instability of fundamental mode. For details see [5]) Fig. 13(a) shows sudden increase in pressure amplitude rising to ~4 kPa due to secondary instability of first harmonic mode. Fig. 14 shows direct flame images at various instants of flame propagation. A curved flame travels downstream and later turns flat due to effect of acoustics. Corrugated structures appear on this flat flame (flames at 0.206-0.208 s) due to the parametric instability leading to rapidly fluctuating flame can be observed. Unlike the fundamental mode at lower S_L conditions described previously, wavelength at onset of parametric instability is lower for higher harmonics and the tube diameter allows the parametric instability. During more rapid flame movement after onset of parametric instability, a rotary motion is observed which changes the rotation direction after a cycle. From 0.243 s to 0.245 s the flame rotates in anticlockwise direction and from 0.247 to 0.249 s the flame rotates in clockwise direction. This cycle is repeated. It can be seen that flame images at 0.244 s and 0.251 s are similar and are a mirror image to that at 0.248 s.

After flame travels around one third of the tube the first harmonic oscillations stop and beating instability of fundamental mode is observed as described in last section. Figure 13(b) shows pressure oscillations during this beating instability for fundamental mode. As noted, secondary instability or parametric instability of fundamental mode is not observed at higher S_L. At S_L=42.5 cm/s, a regime called VI-N is observed. Pressure trace for this regime is shown in Fig. 13 (c) (d). In VI-N, first

harmonic parametric instability happens at the upper part of tube but beating instability is not clearly observed in bottom half, rather a planar flame vibrates at fundamental mode frequency as it propagates downstream as in regime III with primary acoustic instability. On further increasing S_L to 45.0 cm/s, regime N-N is observed where parametric instability of first harmonic is also suppressed which is clear from pressure history in Fig. 13 (e)) where lowering of pressure amplitude to 0.6 kPa is observed. In the bottom part of tube, the flame oscillates as in primary acoustic instability of fundamental mode with weak pressure fluctuations (Fig. 13 (f)). This is an interesting phenomenon where parametric instability of both fundamental mode and first harmonic is suppressed at higher S_L. In contrast, in wider tubes, parametric instability always increases with increasing S_L as more higher modes are observed.

3.4 Effect of *Le*

In this section, some results are presented to understand the effect of *Le* on flame-acoustic instabilities in a narrow tube. Readers should refer to [6][17] [27] for more results on effect of *Le* on flame regimes. First the results with *Le*~1.34 (lean $C_2H_4/O_2/N_2$) (mixture properties in Table 3) are discussed. At S_L=25 cm/s, flame regime IV-N is observed (Fig. 15 (a)) where flame extinguishes soon after parametric instability begins. At S_L=35 cm/s, flame regime similar to regime IV with secondary instability is observed (Fig. 15 (b)). Similar to *Le*=1.05 mixtures, no parametric cells are observed and a counter rotating flame as described in last section are also observed for this *Le*~1.34 and S_L=35 cm/s mixture. The maximum pressure amplitude for regime IV is lower than that for *Le*=1.05. This can be due to lower growth rates of thermoacoustic instability for higher *Le* mixtures as has been shown in our earlier work [5].

On increasing the S_L to 40 cm/s, primary acoustic instability of first harmonic (Fig. 16 (a)) is observed followed by primary acoustic instability of fundamental mode (Fig. 16 (b)). This is clear by the fact that the maximum pressure fluctuation amplitude is around 0.5 kPa which is characteristic of primary acoustic instability. This regime is similar to N-N regime discussed before for *Le*~1.05 mixture or the

beating regime without beating oscillations of fundamental mode. Clear beating oscillations are not observed for this *Le*~1.34 mixture. On further increasing the S_L to 45 and 50 cm/s, similar behavior is observed. The parametric instability is suppressed for both fundamental mode and first harmonic at higher S_L for *Le*=1.34 mixtures. In contrast, for *Le*=1.05 mixtures, parametric instability was observed for first harmonic mode for a range of S_L between 35 and 42.5 cm/s as described in last section.

Now, the results are discussed for *Le*~0.8 mixtures (rich $C_2H_4/O_2/CO_2$) (mixture properties in Table 2). At S_L =11 cm/s, a regime similar to IV-N is observed, where flame transitions to parametric instability and then extinguishes due to heat loss (Fig. 17). The maximum pressure attained before extinction is higher than Le>1 mixtures.

At a higher S_L of 25 cm/s, parametric instability of both first harmonic and fundamental mode can be observed as shown in Fig. 18 (a) and (b) respectively. However, there is a major difference compared with *Le*>1 mixtures. The parametric structures can be clearly observed on flame front as can be seen from images during parametric instability shown in Fig.18. This is similar to parametric structure with just one cell as observed in *Le*-1.05 mixture in tube of inner diameter 2 cm shown in our last work [26].

.

A summary of the flame responses depending on the *Le* is shown in Fig. 19. Parametric cell structures for all harmonics are observed for *L*e=0.8 and in a small range of S_L (35 to 40 cm/s) for first harmonic for *Le*=1.05. Parametric structures are not observed for *Le*=1.34. Hence, *Le* has significant impact on whether parametric structures can be observed in narrow tube experiments due to effect of *Le* on the critical wavelength of parametric instability as discussed in next section. The maximum pressure amplitudes are lower without the emergence of parametric structures. Secondary instability is suppressed at higher S_L for *Le* =1.05. Beating instability is observed only for *Le*=1.05 which

corresponds to CO_2 diluted mixtures. In the next sections we try to understand these phenomena by answering two questions; 1. Why are parametric structures only observed for certain mixtures in a narrow tube? 2. Why beating instability is observed only for *Le*=1.05 mixtures?

3.5 Understanding the emergence and suppression of parametric instability

To summarize, there are three significant observations regarding the parametric instability based on current experiments. First, parametric instability is suppressed at lower diameter as in current experiments as compared with experiments at larger diameter presented in earlier works [5][11]. Second, parametric instability with corrugated structures is easily observed at first harmonic than the fundamental mode. Third, parametric instability of all harmonics is suppressed at higher S_L. To explain these observations, first we provide a brief explanation of the theory of parametric instability. Fig. 20 shows the stability of a planar flame front in acoustic field. This theory has been successful in explaining the features of parametric instability in propagating flames in tubes [6]. Parametric instability is generated if the acoustic velocity reaches a critical value. Then parametric cell structures of a particular wavenumber are generated on the flame front. Naturally, two conditions arise for generation of parametric instability. First, the acoustic velocity fluctuations should reach the critical value. Second, the geometry of combustion chamber should allow the formation of parametric cells.

Theoretical predictions are performed to explain the trends observed in experiments. The calculation method is discussed in detail in our last work [6]. Figure 21 (a) shows effect of frequency on wavelength of parametric instability. The wavelength of fundamental mode (90 Hz) is higher than that for first harmonic mode (270 Hz). Parametric structures of first harmonic were observed in experiments for which the wavelength (~0.39 cm) is just below half the tube diameter. Parametric structures for fundamental mode were not observed because the critical wavelength (~0.6 cm) is higher than half the tube diameter. If the tube diameter is more than twice the critical wavelength then parametric structures can be clearly observed as in our past experiments. For same *Le*~1.05 mixtures,

parametric structures were observed for tube diameter of 2 cm [27] and higher [6]. This explains the first and second observation. Based on this discussion, following criteria can be proposed for occurrence of parametric structures

$D \geq 2\lambda_{parametric}$ (1)

This condition is schematically shown in Fig. 22. For tube geometry the diameter should be greater than the wavelength of parametric instability. For Hele-Shaw cells, maximum of plate width and gap width should be greater than twice the wavelength of parametric instability as shown in Fig. 22. This condition will usually be satisfied in a typical Hele-Shaw cell experiment hence parametric instability would be suppressed if the acoustic velocity could not reach the critical amplitude. This could happen due to high acoustic losses if the gap width is very small.

Figure 21 (b) shows the variation of acoustic velocity with S_L for *Le*=1.05. It can be seen that there is a minimum for critical acoustic velocity near 20 cm/s and 35 cm/s for fundamental and first harmonic modes. In experiments, secondary instability was observed near these minimums. At higher S_L, the critical acoustic velocity needed to initiate parametric instability is higher making it difficult for the parametric instability to be generated at higher S_L. This explains the third observation.

At this point it is important to clarify why it is easier to generate parametric instability in wider tubes even at higher S_L. In fact, the tendency to generate parametric instability increases with S_L as higher modes of parametric instability are also activated. As noted earlier, parametric instability happens when U_a reaches a critical value and parametric structure of certain wavelength is observed provided that Eq. 1 is satisfied. Now, in wider tubes Eq. 1 is easily satisfied, so that is not an issue. Also, due to lower acoustic losses the critical U_a is reached easily even at higher S_L, giving rise to the instability. Effect of diameter and frequency on acoustic losses is discussed below.

Acoustic losses: Two kinds of acoustic losses are usually considered for thermoacoustic instability of flames propagating in tubes [4]; acoustic radiation loss from the open end of the tube ($\frac{1}{\tau_{rad}}$) and wall losses due to boundary layer ($\frac{1}{\tau_{wall}}$). Total acoustic loss ($\frac{1}{\tau_{loss}}$) is sum of these losses

$$\frac{1}{\tau_{loss}} = \frac{1}{\tau_{rad}} + \frac{1}{\tau_{wall}} = \frac{1}{8}\frac{(\omega D)^2}{cL} + \sqrt{8}\frac{(\omega\alpha)^{1/2}}{D}[(\gamma-1)/\sqrt{\gamma} + \sqrt{Pr}] \quad (2)$$

Here, ω is circular frequency, $2\pi f$, f, being the measured frequency; D, L are diameter and length of tube (702 mm); α is thermal diffusivity; γ is ratio of specific heats; Pr is Prandtl number. Variation of total losses with the diameter of tube and the acoustic frequency is shown in Fig. 23. Radiation losses increase with diameter and wall losses decrease with diameter. Both losses increase with increasing frequency. Hence, higher harmonics are subjected to higher acoustic losses and are more effectively damped which is one of the reasons why higher harmonic instabilities are observed at higher S_L. Acoustic radiation losses are negligible for low diameter tubes and the loss is influenced only by wall losses. Total acoustic losses increase significantly with decreasing diameter. Acoustic loss increases ten-fold when diameter decreases from 3 cm to 0.8 cm. Hence, instability in tubes with diameter more than ~ 3 cm are very less affected by acoustic losses but for tubes with diameter below 1 cm acoustic losses are a major factor. Hence, parametric instability can be easily generated in wider tubes. Due to higher acoustic losses, maximum pressure also decreases with tube diameter [5]. Effect of diameter on maximum pressure and growth rates of primary and secondary instability has been measured and discussed in detail in our recent work [27].

Finally, it is noted that the parametric instability occurs due to the time-dependent acceleration produced by the acoustic wave through the mechanism of Raleigh-Taylor Instability. This influence can be characterized by inverse of effective Froude number as was noted by Searby and Roechwerger [3]and discussed by Petchenko et al. [28].

$$\frac{1}{Fr} = \omega\tau\frac{U_a}{S_L} \quad (3)$$

Here U_a is amplitude of acoustic velocity fluctuation. Non-dimensional frequency, ωτ is ratio of chemical time scale, $\tau = \frac{D_1}{S_L^2}$, to acoustic time scale $\frac{1}{\omega}$. It can be easily seen that acceleration effect and thus tendency for parametric instability is higher for higher frequency and lower S_L consistent with our earlier discussion.

Figure 24 shows the effect of *Le* on features of parametric instability. It can be seen that the wavelength at onset of parametric instability increases with *Le*. Thus, the criterion of Eq. 1 can be satisfied for *Le* ~0.8 mixtures at lower diameters than that for *Le* ~1.05 and 1.34 mixtures. Also, the critical acoustic velocity required for generation of parametric instability is lower for lower *Le*. For *Le*~1.34 mixtures the critical wavelength doesn't satisfy Eq. 1 for both fundamental mode and first harmonic (wavelength = 0.61 cm) hence parametric structures are not observed for either modes. The generation of parametric instability is easier for lower *Le* mixtures which is consistent with experimental observations.

3.6 Discussion on effect of heat losses and beating instability

A beating instability had been reported for a burner stabilized flame in the Rijke tube near the limit of operation in terms of equivalence ratio and flow rates of fuel and air [29]. They argue that non-linear interaction of pulsating instability of flat flame caused by conductive heat losses to the burner rim with acoustic instability creates the beating instability. Here, the beating instability can also be caused by similar interaction where pulsating instability is generated due to various heat losses. The spinning motion of flames observed here (Fig. 14) is also a signature of pulsating instability [25]. Joulin and Clavin [24] theoretically predicted an oscillatory behavior of planar flames of *Le*>1 called pulsating instability if experiments are performed in cooled annular burners of width slightly greater than quenching distance with adequate mixtures. Higher heat losses can reduce the critical *Le* for which such pulsating instability can be observed. Current tube diameter of 8 mm is also slightly higher than the quenching diameter and there is a good possibility that pulsating instability can be obtained due to higher heat losses due to both convection and radiation.

Beating instability was observed only for CO_2 diluted *Le*=1.05 mixtures in current experiments. Based on the experimental observations and above discussion, our hypothesis is that three conditions are required for the beating instability to occur 1. *Le*≥1.0, such that flame is capable of exhibiting pulsating instability 2. Parametric instability should be suppressed. 3. Primary instability should occur so that flame is oscillating at an acoustic frequency.

For *Le* = 0.8 mixtures, parametric instability could be easily generated for various S_L because the characteristic wavelength at the onset of parametric instability satisfies Eq. 1. Suppression of parametric instability is necessary for this beating to occur. So, beating could not be observed with *Le*=0.8 mixtures.

These conditions are apparently satisfied by *Le*~1.34 mixtures which are N_2 diluted as seen in section 3.4 but beating is not observed as in *Le*~1.05 mixtures with CO_2 dilution. Our hypothesis is that radiation heat losses can cause pulsating instability in the CO_2 diluted mixtures because CO_2 and H_2O which are radiating species comprise more than 90% of burnt gases in these mixtures. So, next, we analyze the heat losses which also cause flame extinction observed in certain mixtures (regime IV-N).

Heat losses: In a first approximation, the heat loss rate, q_l to the wall by convection can be approximated as,

$$q_l = h(\pi D\delta)(T_b - T_u) \tag{4}$$

Here h is heat transfer coefficient, D is diameter of tube, δ is the thickness of flame brush, T is temperature and the subscripts b and u refer to burnt and unburnt mixtures. h can be found if Nusselt number, Nu is known, through the relation $h = Nuk_g/D$, where k_g is thermal conductivity of mixture. Nu can be approximated as 4.0 which is between Nu for constant temperature boundary condition and constant wall heat flux boundary condition for a circular tube. Such Nu has also been found appropriate to model convective heat loss during combustion in small diameter tubes[30]. Heat released by combustion, q_r can be approximated as

$$q_r = \rho\left(\frac{\pi D^2}{4}\right) S_L C_p (T_b - T_u). \tag{5}$$

Comparative importance of these rates can be understood by taking their ratio

$$\frac{q_l}{q_r} = 16\frac{k_g\delta}{\rho S_L C_p D^2} = 16(\frac{\delta}{D})^2 \quad (6)$$

For mixtures used in current work, theoretical flame thickness is typically around 0.008 cm and the tube diameter is 0.8 cm. So, the ratio of heat loss to heat generation evaluates to $1.6\text{x}10^{-3}$. Similar analysis was performed recently by[19]. They conclude that the heat loss plays a negligible role if characteristic width is near 1 cm. The flame thickness decreases with increasing burning velocity. So, convective heat loss will be more important factor at low burning velocity. It should also be noted that this analysis is done considering a steady planar flame which would be good approximation even for slightly curved flame or flame undergoing primary instability where nearly flat flame is observed. But, in the situations where flame undergoes secondary instability, the planar flame thickness no longer remains the governing parameter. Depending on the flame oscillation amplitude, effective flame thickness can be larger and thus effective heat loss will also be larger. Indeed, the effect of heat loss is clearly observed for S_L of 15 cm/s for *Le*=1.05. Flame can easily propagate until the saturation of primary instability but when the secondary instability begins and flame area is increased the flame is extinguished. When S_L increases to 20 cm/s heat release seems enough to sustain the flame even with higher oscillation amplitudes. Similar effect of heat losses is also observed at other *Le* leading to flame extinction at the onset of parametric instability.

Radiative heat loss can also be important in current $C_2H_4/O_2/CO_2$ mixtures because CO_2 and H_2O which are major radiating gases constitute more than 90% of the combustion products. For usual fuel/air mixture, the fraction of radiating species is an order of magnitude lower. The simplest approximation of the radiative heat losses from combustion gases can be done using Hottel charts described in standard textbooks [31] and is given as

$$q_{rad} = \sigma A \varepsilon_g (T_b^4 - T_{amb}^4) \quad (7)$$

ε_g can be estimated using Hottel charts and is found to be around 0.014 for CO_2 mixed with other non-radiating species at T_b of 2100 K and for CO_2 concentration in mixture of S_L around 30 cm/s in a long tube of inner diameter 8 mm. Effect of radiation from other species are neglected. The species

concentrations in burnt gas are calculated assuming a freely propagating flame with CHEMKIN using detailed kinetic model of USC II mechanism. The subscript amb refers to ambient. A is the total flame surface area and taken as cross section area of the tube as a first approximation. This approximation is reasonable because the curved area of a cylindrical flame (its height = flame thickness) is negligible and if we assume that one side of the flame is at same temperature as that of the flame, the total area can be approximated as the cross-section area of the tube. In this case, the ratio of radiative heat loss to heat release $\frac{q_{rad}}{q_r}$ is estimated to be 0.02. This is larger than the conductive heat losses by around an order of magnitude even though radiation from other species are not considered. Moreover, radiation reabsorption would reduce radiative heat loss [32] and it is also known that Hottel Charts method slightly overestimates the radiative heat loss [33][34]. Nonetheless, it can be concluded that radiative heat loss can be important in current CO_2 diluted mixtures. Combined radiation and conduction heat loss in a narrow tube near quenching diameter give similar fractional heat loss parameter as is reported in previous modeling of beating instability [29] and are sufficient to cause pulsating instability for current mixtures with *Le* = 1.05 in diameters near the quenching diameter. Pulsating instability due to radiative heat losses in rich hydrogen-air flames have also been predicted earlier [35].

For *Le* = 1.34 mixtures, the suppression of parametric instability is observed for all harmonics as seen in Section 3.4 but the heat losses are not enough to cause pulsating instability. This can be because the mixture is diluted with N_2 where the concentration of radiating gas CO_2 is an order of magnitude lower than CO_2 diluted mixtures and thus the radiation heat loss is also much lower. The lower heat loss condition couldn't generate favorable situation for pulsating instability thus beating is also not observed even though the *Le* of 1.34 is slightly higher than *Le* of 1.05 where beating is observed. It should be noted that pulsating instability was reported for *Le*=1.86 in N_2 diluted $C_3H_8/O_2/N_2$) mixtures [26]. It is thought that this beating instability can be observed in narrow combustion tubes given the mixture conditions are conducive for pulsating instability i.e. mixtures with sufficiently high *Le* or appropriate heat loss. In future, further experiments and numerical studies can be performed to prove or disprove this hypothesis and predict the instability presented in this work.

4. Conclusion

Thermoacoustic instability of downward propagating flame in a narrow tube of inner diameter 8 mm was examined. Some new flame regimes specific to narrow tubes were identified. For e.g. extinction of flames was observed soon after onset of secondary acoustic instability. Secondary acoustic instability and the parametric instability of flame front were suppressed for fundamental mode at S_L higher than 22.5 cm/s. A beating instability was observed for 25.0 cm/s $\leq S_L \leq$ 40.0cm/s. It is argued that this beating instability can be due to interaction of pulsating instability of flame with thermoacoustic instability where the pulsating instability of planar flame can be caused by combined convective and radiative heat losses. This argument was further supported by the fact that beating was not observed for mixtures with $Le<1$ as well as mixtures with $Le>1$ where radiation heat loss is not significant. Dependence of parametric instability on tube diameter, Le, S_L and frequency was clarified.

Acknowledgements

This study was supported by a Grant-in-Aid for Scientific Research (KIBAN(A)#18H03755) from MEXT Japan. This study was also supported by JSPS KAKENHI Grant number JP20K22382, a Grant-in-Aid for Research Activity Start-up.

References

[1] H. Guenoche, Non-steady Flame Propagation, G. H. Markstein, Ed. Pergamon, 107–181.

[2] G. Searby, Acoustic Instability in Premixed Flames, Combust. Sci. Technol., 81 (1992) , 221–231.

[3] G. Searby, D. Rochwerger, A parametric acoustic instability in premixed flames, J. Fluid Mech., 231 (1991) , 529–543.

[4] C. Clanet, G. Searby, P. Clavin, Primary acoustic instability of flames propagating in tubes: cases of spray and premixed gas combustion, J. Fluid Mech., 385 (1999) , 157–197.

[5] A. K. Dubey, Y. Koyama, N. Hashimoto, O. Fujita, Experimental and theoretical study of secondary acoustic instability of downward propagating flames: Higher modes and growth rates, Combust. Flame, 205 (2019) , 316–326.

[6] A. K. Dubey, Y. Koyama, S. H. Yoon, N. Hashimoto, O. Fujita, Range of "complete" instability of flat flames propagating downward in the acoustic field in combustion tube: Lewis number effect, Combust. Flame, 216 (2020) , 326–337.

[7] P. Clavin, P. Pelcé, L. He, One-dimensional vibratory instability of planar flames propagating in tubes, J. Fluid Mech., 216 (1990) , 299–318.

[8] A. C. Mcintosh, Pressure disturbances of Different Length Scales Interacting with Conventional Flames, Combust. Sci. Technol., 75 (1991) , 287–309.

[9] P. Clavin, G. Searby, Unsteady response of chain-branching premixed-flames to pressure waves, Combust. Theory Model., 12 (2008) , 545–567.

[10] P. Pelcé, D. Rochwerger, Vibratory instability of cellular flames propagating in tubes, J. Fluid Mech., 239 (1992) , 293–307.

[11] A. K. Dubey, Y. Koyama, N. Hashimoto, O. Fujita, Effect of geometrical parameters on thermo-acoustic instability of downward propagating flames in tubes, Proc. Combust. Inst., 37 (2019) , 1869–1877.

[12] S. H. Yoon, T. J. Noh, O. Fujita, Onset mechanism of primary acoustic instability in downward-propagating flames, Combust. Flame, 170 (2016) , 1–11.

[13] Y. Taniyama, O. Fujita, Initiation and formation of the corrugated structure leading to the self-turbulization of downward propagating flames in a combustion tube with external laser absorption, Combust. Flame, 161 (2014) , 1558–1565.

[14] Y. Chung, O. Fujita, N. Hashimoto, Effect of Le on criteria of transition to secondary acoustic instability of downward-propagating flame in a tube with controlled curvature induced by external laser, Proc. Combust. Inst., (2018) .

[15] M. Tsuchimoto, O. Fujita, T. Honko, Y. Nakamura, H. Ito, Research on the relation of flame front curvature and oscillatory flame propagation by external laser irradiation method, Proc. Combust. Inst., 32 (2009) , 1003–1009.

[16] J. S. Park, O. Fujita, Y. Nakamura, H. Ito, Transition of flat flames to turbulent motion induced by external laser irradiation, Proc. Combust. Inst., 33 (2011) , 1105–1112.

[17] S. H. Yoon, T. J. Noh, O. Fujita, Effects of Lewis number on generation of primary acoustic instability in downward-propagating flames, Proc. Combust. Inst., 36 (2016) , 1603–1611.

[18] R. C. Aldredge, N. J. Killingsworth, Experimental evaluation of Markstein-number influence on thermoacoustic instability, Combust. Flame, 137 (2004) , 178–197.

[19] F. Veiga-López, D. Martínez-Ruiz, E. Fernández-Tarrazo, M. Sánchez-Sanz, Experimental analysis of oscillatory premixed flames in a Hele-Shaw cell propagating towards a closed end, Combust. Flame, 201 (2019) , 1–11.

[20] F. J. Higuera, Acoustic response of a lean premixed flame propagating upward in a tube, Combust. Flame, 199 (2019) , 377–386.

[21] Y. Ju, K. Maruta, Microscale combustion: Technology development and fundamental research, *Progress in Energy and Combustion Science*, 37 (2011) . 669–715, Dec-2011.

[22] K. Maruta, Micro and mesoscale combustion, Proc. Combust. Inst., 33 (2011) , 125–150.

[23] F. Veiga-López, M. Kuznetsov, D. Martínez-Ruiz, E. Fernández-Tarrazo, J. Grune, M. Sánchez-Sanz, Unexpected Propagation of Ultra-Lean Hydrogen Flames in Narrow Gaps, Phys. Rev. Lett., 124 (2020) , 174501.

[24] G. Joulin, P. Clavin, Linear stability analysis of nonadiabatic flames: Diffusional-thermal model, Combust. Flame, 35 (1979) , 139–153.

[25] H. Pearlman, Excitability in high-Lewis number premixed gas combustion, Combust. Flame, 109 (1997) , 382–398.

[26] S. H. Yoon, L. Hu, O. Fujita, Experimental observation of pulsating instability under acoustic field in downward-propagating flames at large Lewis number, Combust. Flame, 188 (2018) , 1–4.

[27] A. K. Dubey, Y. Koyama, N. Hashimoto, O. Fujita, Exploring a critical diameter for thermo-acoustic instability of downward propagating flames in tubes, Proc. Combust. Inst., 38 (2021) .

[28] A. Petchenko, V. Bychkov, V. Akkerman, L. E. Eriksson, Violent folding of a flame front in a flame-acoustic resonance, Phys. Rev. Lett., 97 (2006) , 164501.

[29] F. Weng, S. Li, D. Zhong, M. Zhu, Investigation of self-sustained beating oscillations in a Rijke burner, Combust. Flame, 166 (2016) , 181–191.

[30] K. Maruta, T. Kataoka, N. Il Kim, S. Minaev, R. Fursenko, Characteristics of combustion in a narrow channel with a temperature gradient, Proc. Combust. Inst., 30 (2005) , 2429–2436.

[31] F. P. Incropera, P. DeWitt, David, L. Bergman, Lavine, A. S., *Fundamentals of Heat and Mass Transfer, 6th Edition*. .

[32] Y. Ju, G. Masuya, P. D. Ronney, Effects of radiative emission and absorption on the propagation and extinction of premixed gas flames, Symp. Combust., 27 (1998) , 2619–2626.

[33] Y. Ju, H. Guo, F. Liu, K. Maruta, Effects of the Lewis number and radiative heat loss on the bifurcation and extinction of CH 4 /O 2-N 2-He flames, J. Fluid Mech, 379 (2019) , 165–190.

[34] C. L. Tien, S. C. Lee, Flame radiation, Prog. Energy Combust. Sci., 8 (1982) , 41–59.

[35] E. . Christiansen, C. . Law, C. . Sung, Steady and pulsating propagation and extinction of rich hydrogen/air flames at elevated pressures, Combust. Flame, 124 (2001) , 35–49.

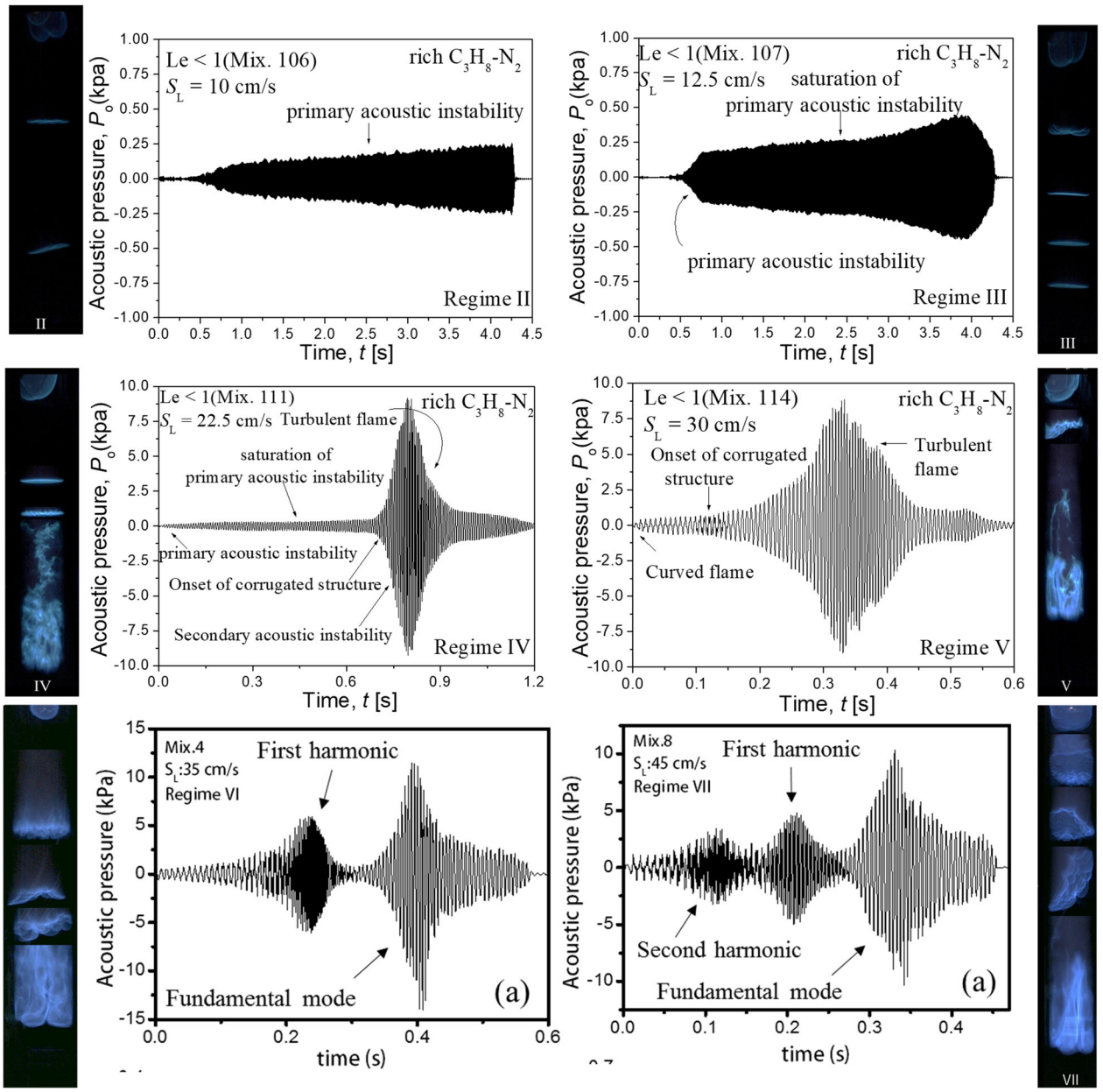

Fig. 1. Flame shapes and pressure fluctuations of regimes II, III, IV, V (taken from [6]) and regime VI, VII (taken from[5]) showing thermoacoustic instability. More details can be found in these references.

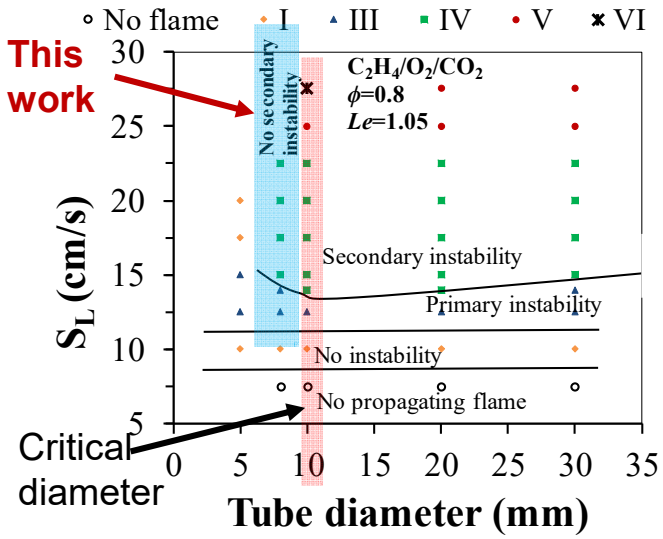

Fig. 2. Experimental conditions targeted in this work in relation to critical diameter. The figure is taken from [27].

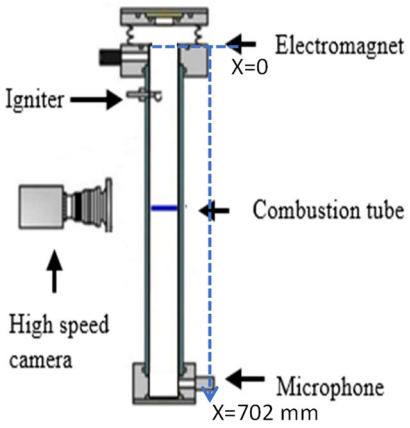

Fig.3. Schematic of experimental setup. Distance is measured from open end of the tube.

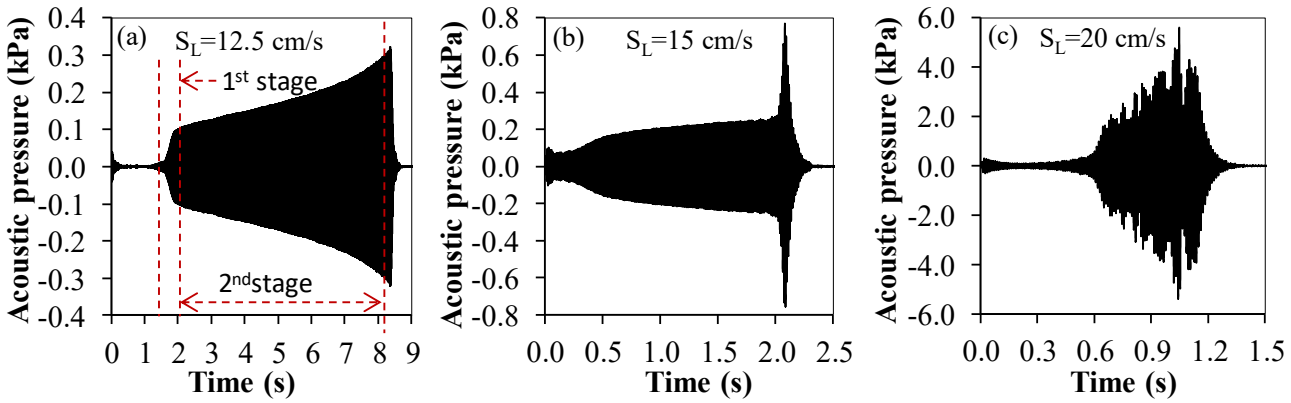

Fig. 4. Pressure fluctuations during thermoacoustic instability at S_L=12.5 cm/s (regime III), 15 cm/s (regime IV-N) and 20 cm/s (regime IV) for *Le*~1.05 mixture.

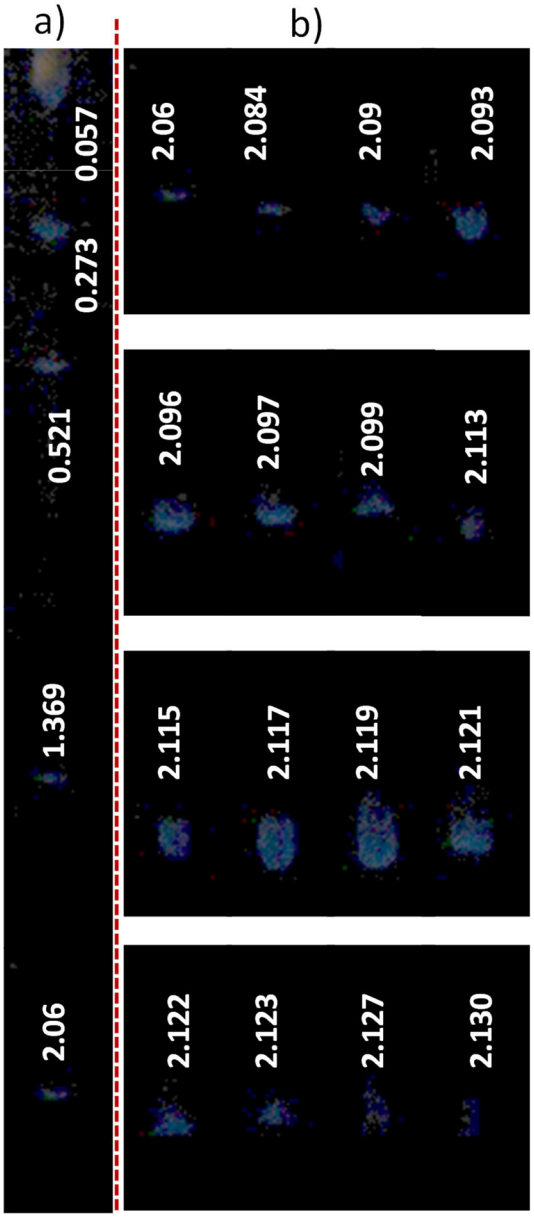

Fig. 5. Flame images at various times during regime IV-N, S_L=15.0 cm/s a) shows top 20 cm of the tube b) shows 15.5 cm to 20 cm from top where flame extinction occurs. The numbers indicate time in seconds from the ignition.

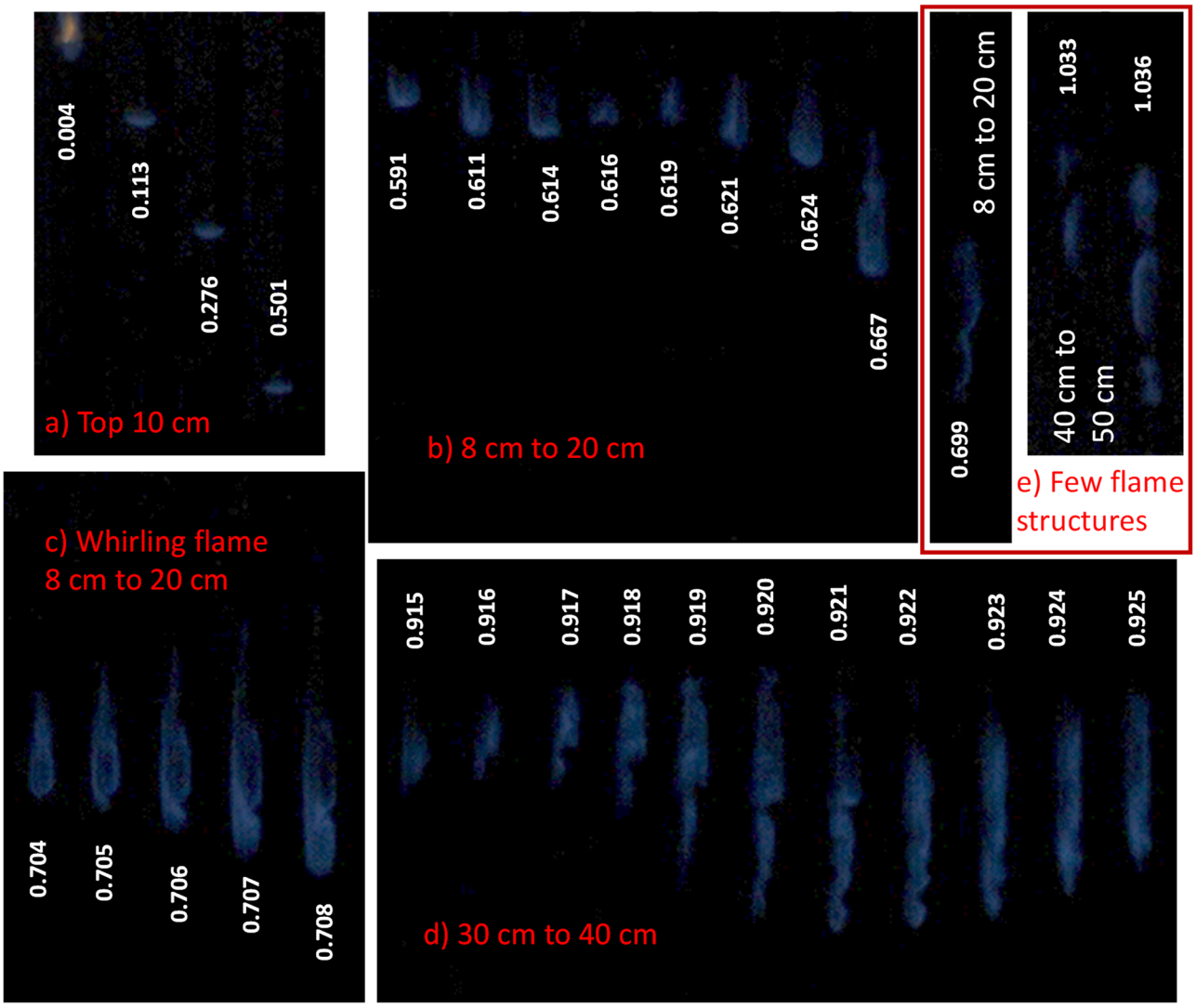

Fig. 6. Flame images at various instances of flame propagation during regime IV at S_L=20.0 cm/s a) shows top 10 cm of the tube, b) shows section from 8 cm to 20 cm from top c) shows tube section from 8 cm to 20 cm d) shows tube section from 30 to 40 cm from top, e) shows some peculiar flame structures during flame propagation. The numbers indicate time in seconds from the ignition.

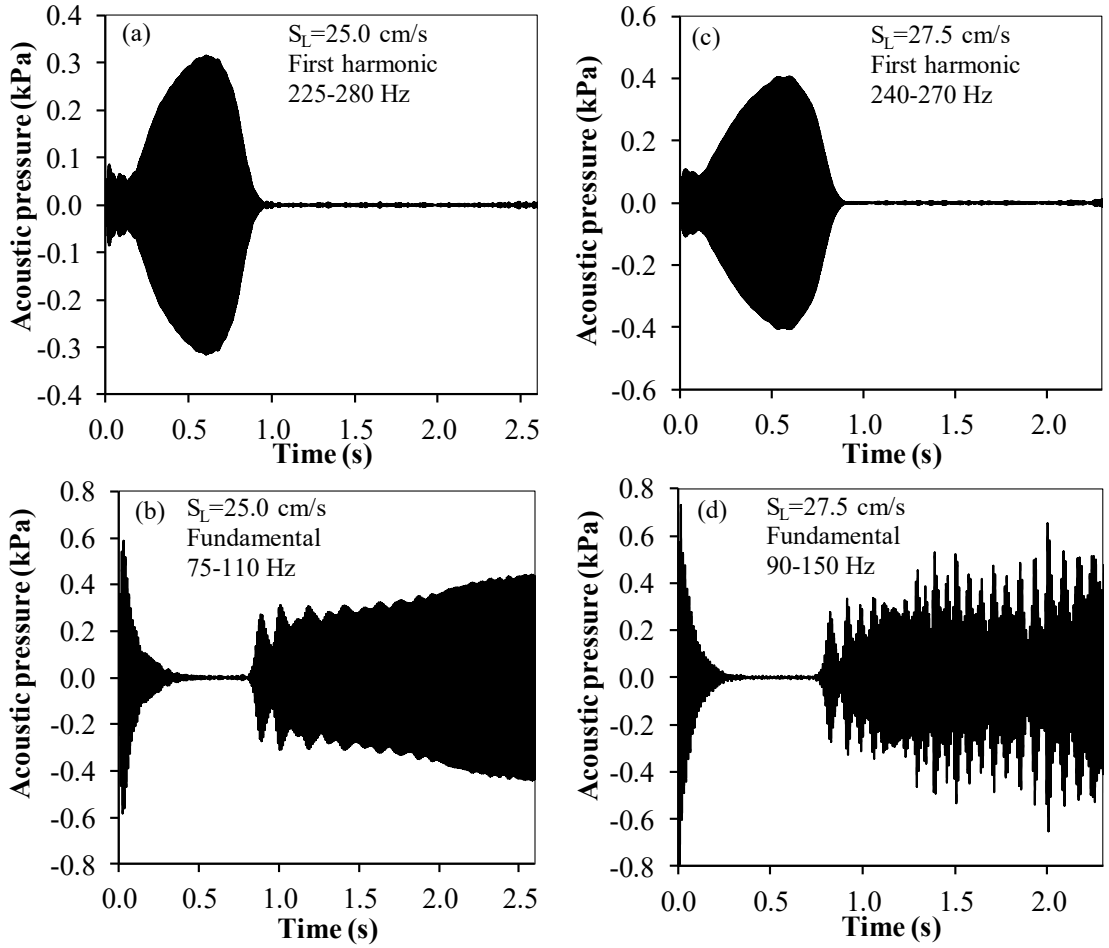

Fig.7. Fundamental and first harmonic pressure oscillations at S_L =25 cm/s and 27.5 cm/s.

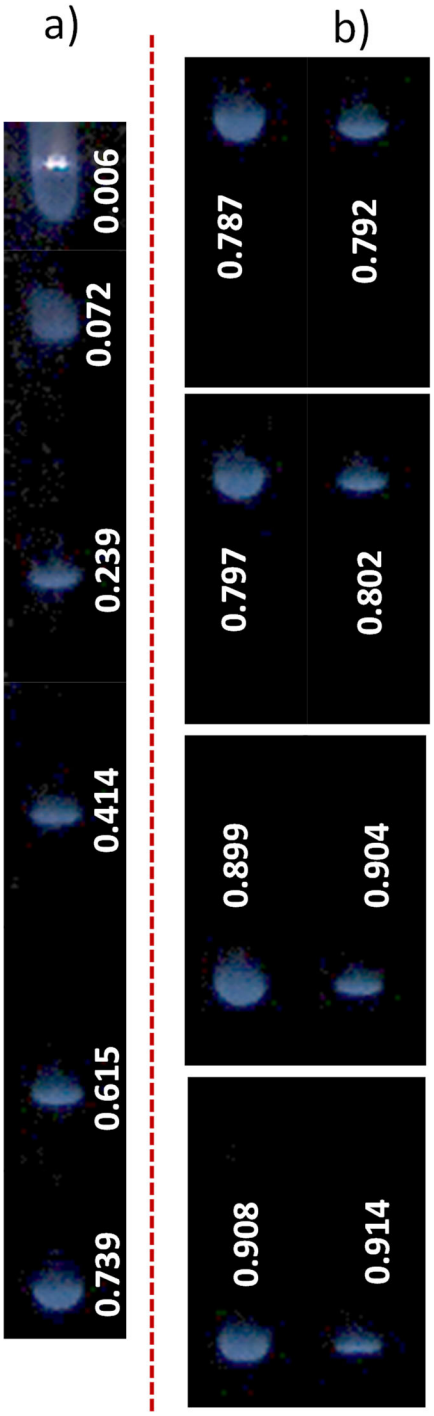

Fig. 8. Flame images at various instances of flame propagation during beating regime at S_L=27.5 cm/s a) shows top 18.5 cm of the tube where flame oscillates at first harmonic b) shows 18.5 cm to 23.5 cm from top where beating can be observed. The numbers indicate time in seconds from the ignition.

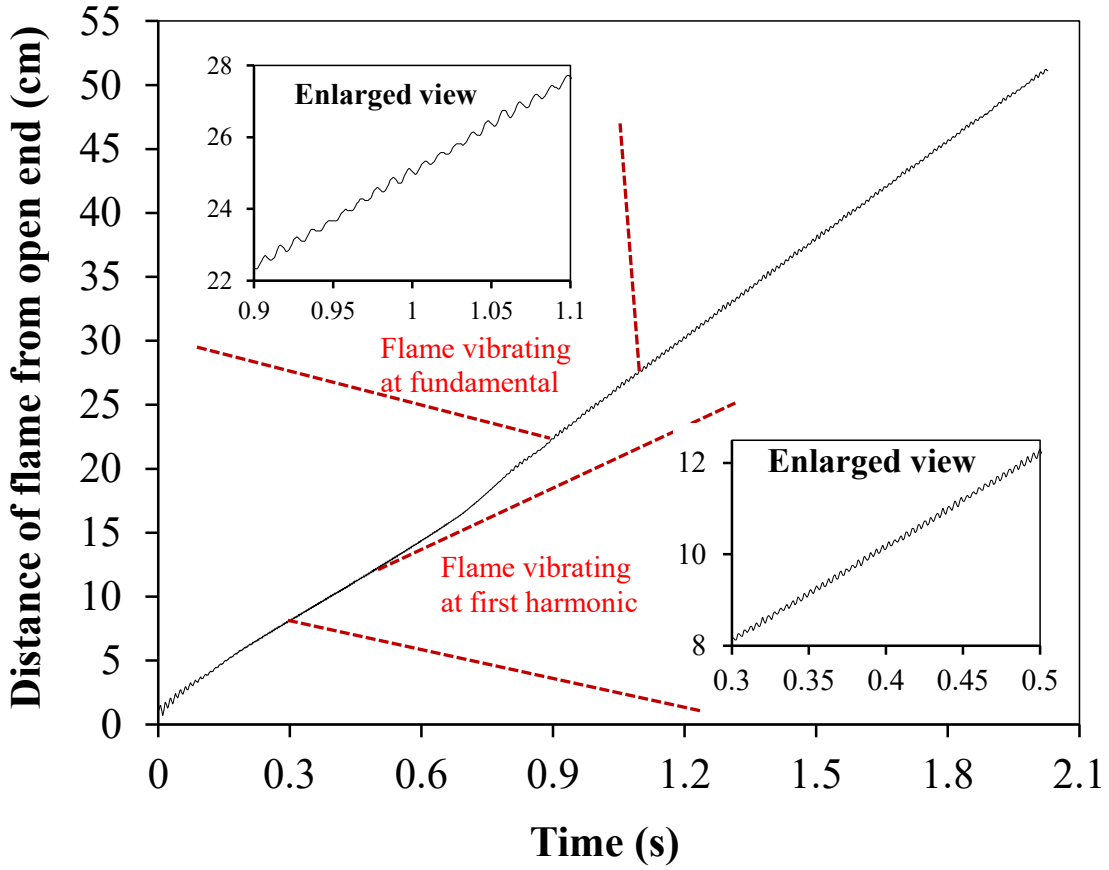

Fig. 9. Flame front time history showing flame oscillation at S_L=27.5 cm/s. Enlarged views of periods when flames vibrate at fundamental mode and first harmonic are also shown.

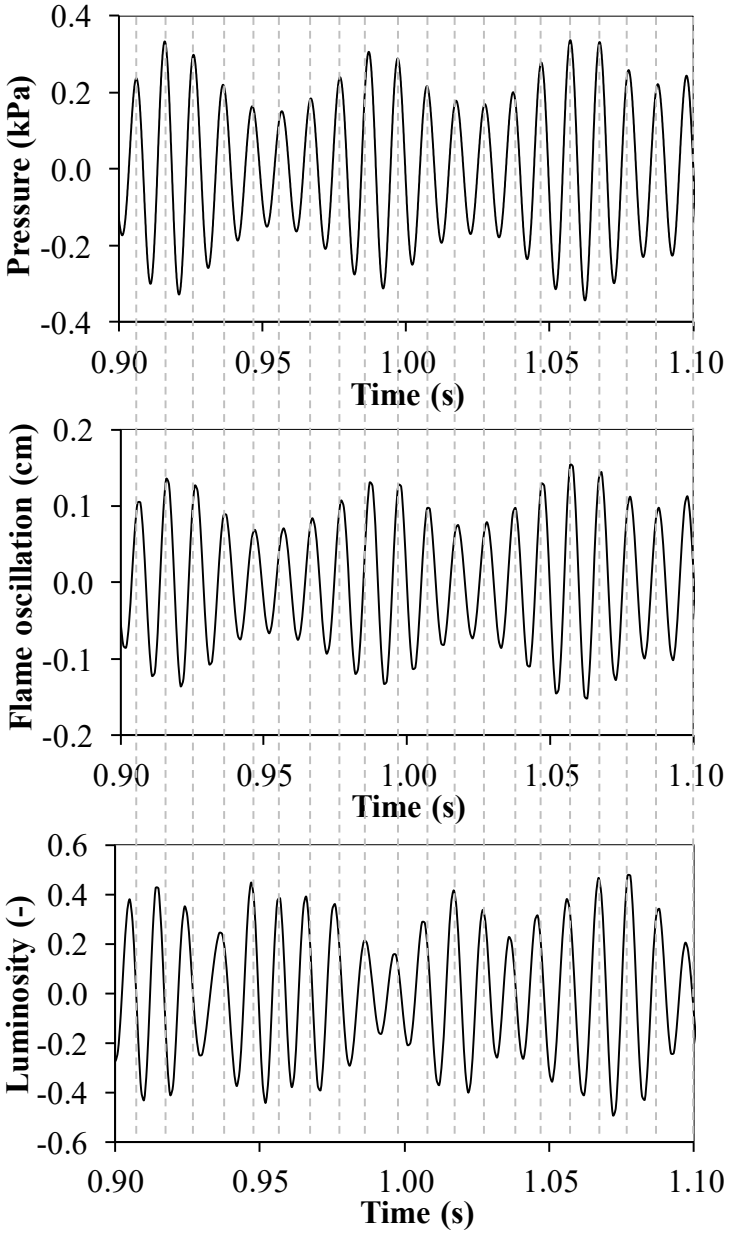

Fig.10. Variation of pressure, flame position and luminosity during beating instability at S_L=27.5 cm/s.

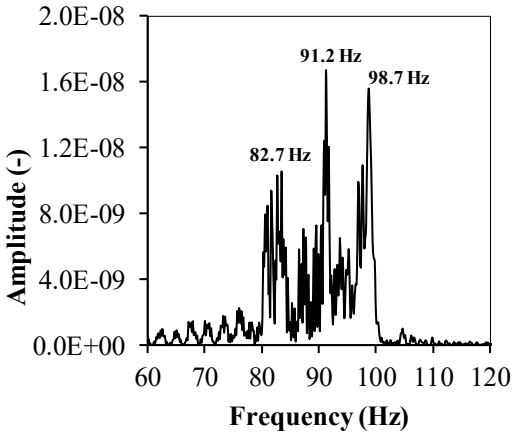

Fig. 11. Dominant frequencies at S_L=27.5 cm/s.

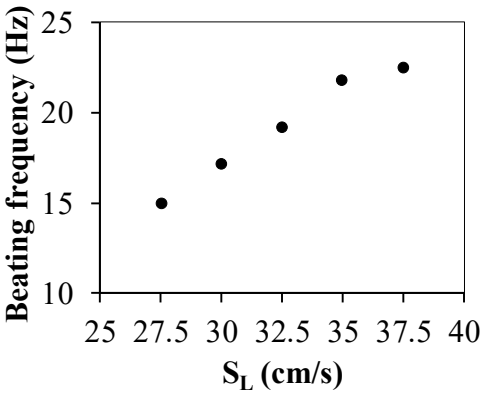

Fig.12. Beating frequency at various S_L.

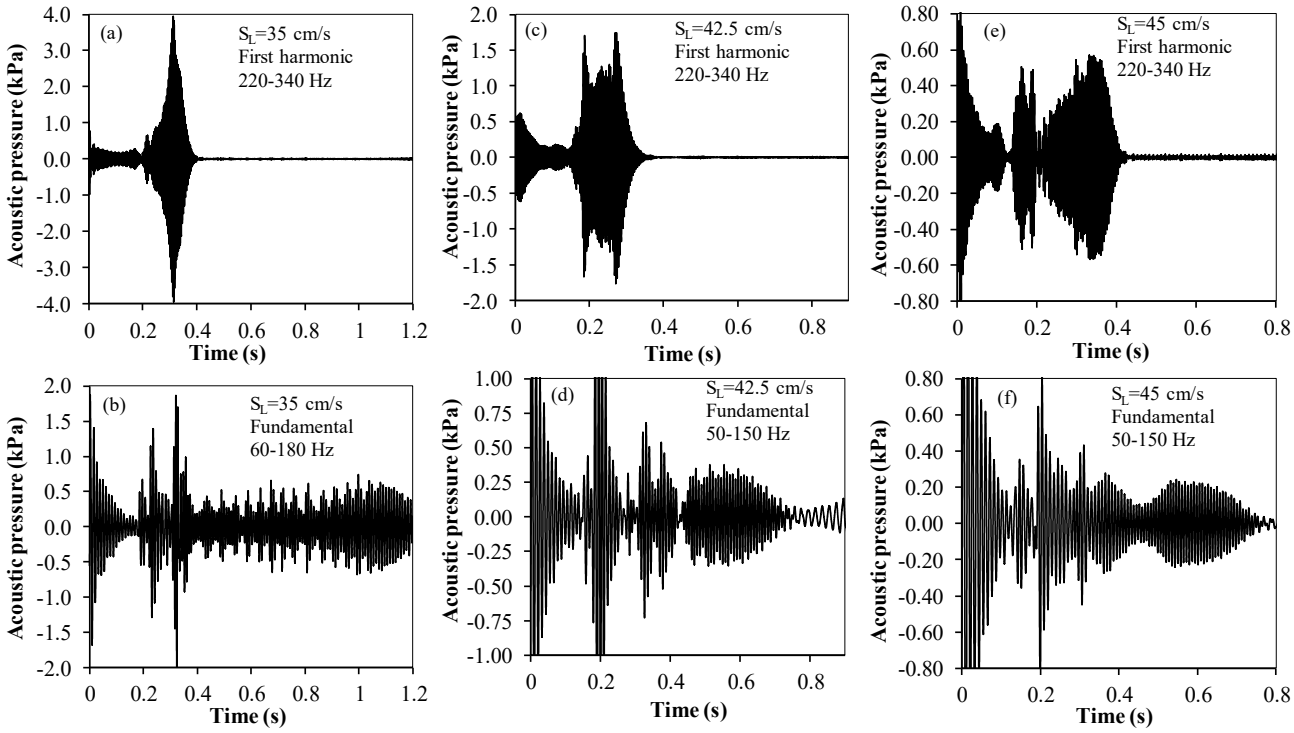

Fig.13. Fundamental and first harmonic pressure oscillations at S_L =35 cm/s regime VI-beating, 42.5 cm/s regime VI-N and 45 cm/s regime N-N.

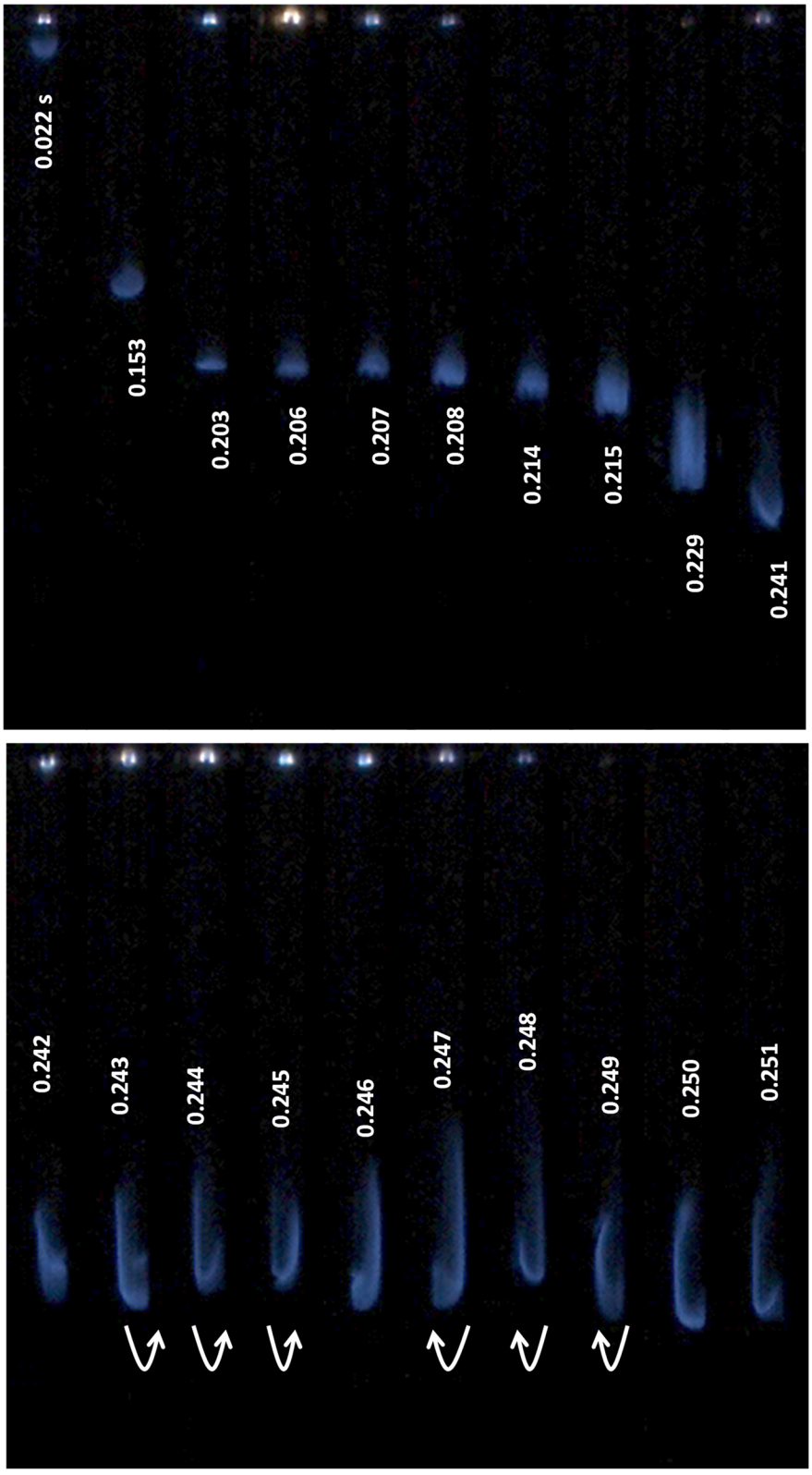

Fig. 14. Flame images at various instances showing corrugations on the flame front during parametric instability of first harmonic and rotating flame front during regime VI-N at S_L=35.0 cm/s Top 18.5 cm of the tube is shown. Time in seconds from ignition is also noted.

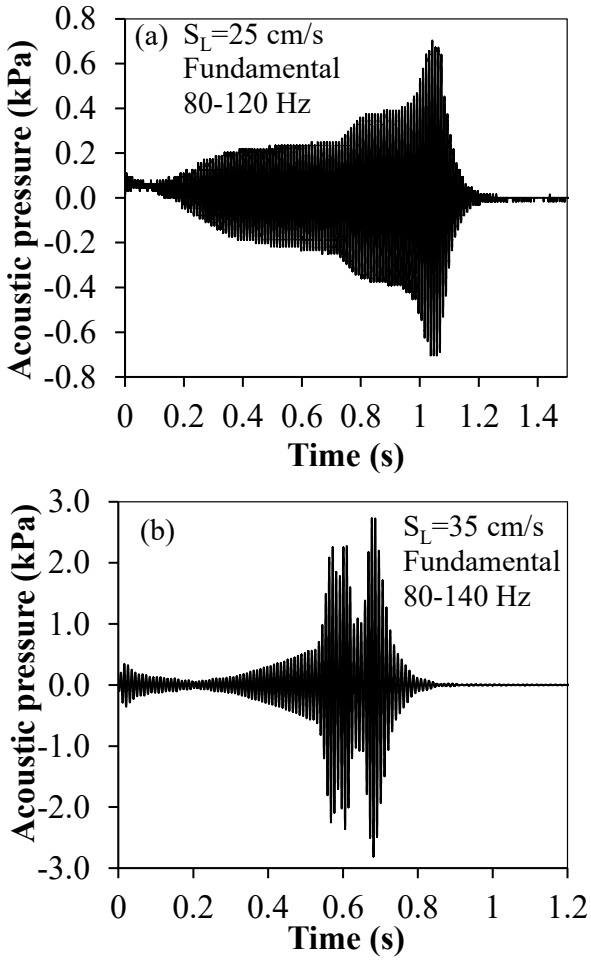

Fig.15. Pressure fluctuations during thermoacoustic instability at S_L=25.0 cm/s (IV-N) and 35.0 cm/s (IV) for *Le*~1.34.

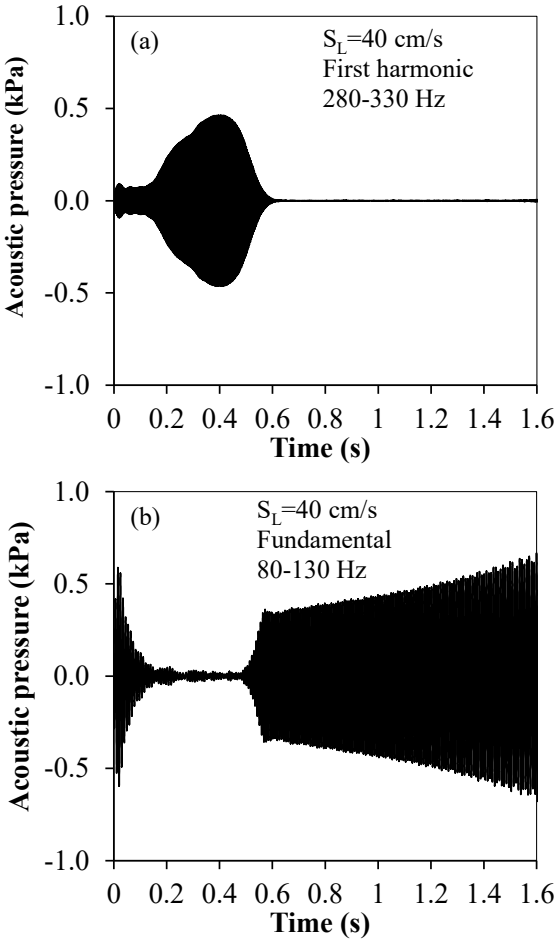

Fig. 16. First harmonic and fundamental mode pressure oscillations at S_L=40 cm/s for *Le* ~1.34 ($C_2H_4/O_2/N_2$).

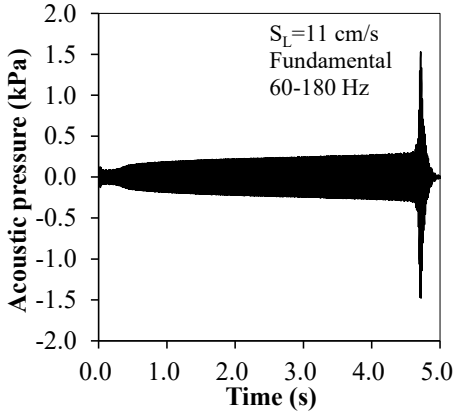

Fig. 17. Pressure fluctuations during thermoacoustic instability at S_L=11.0 cm/s (IV-N) for *Le*~0.8 (rich $C_2H_4/O_2/CO_2$).

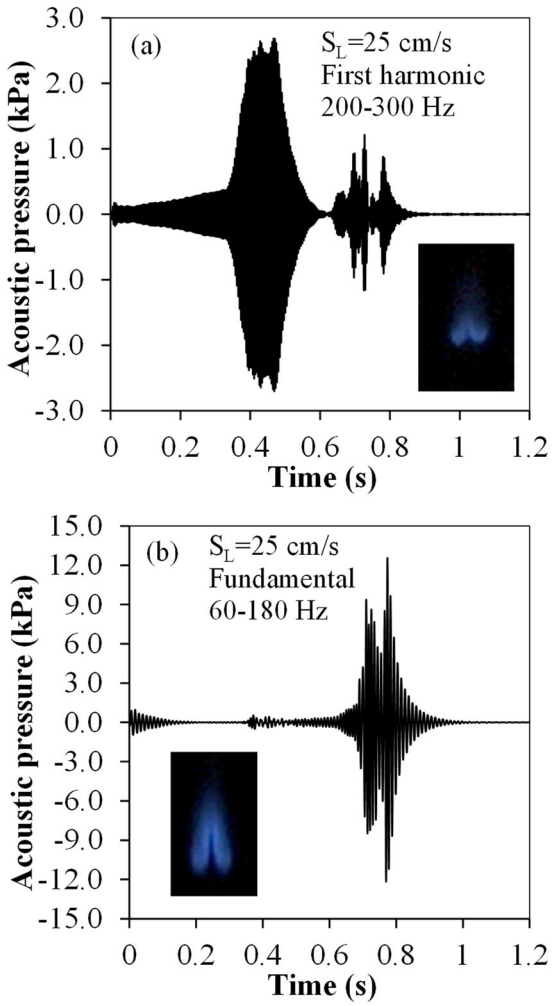

Fig. 18. First harmonic and fundamental mode pressure oscillations at S_L=25 cm/s for *Le*=0.8 (rich $C_2H_4/O_2/CO_2$). Parametric structures at flame front are also shown

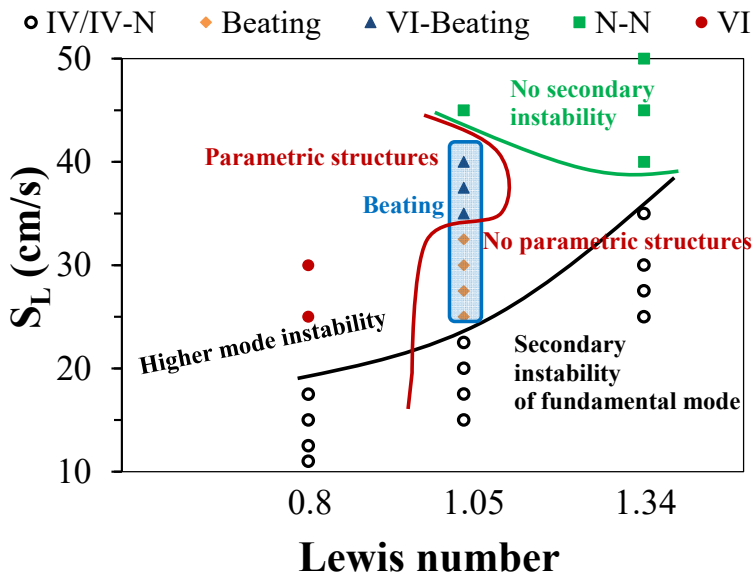

Fig. 19. Summary of flame responses with Lewis number.

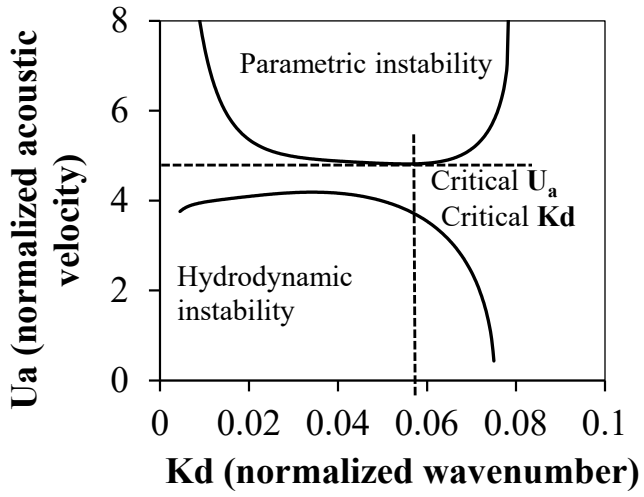

Fig. 20. Stability regimes of a planar flame in acoustic field

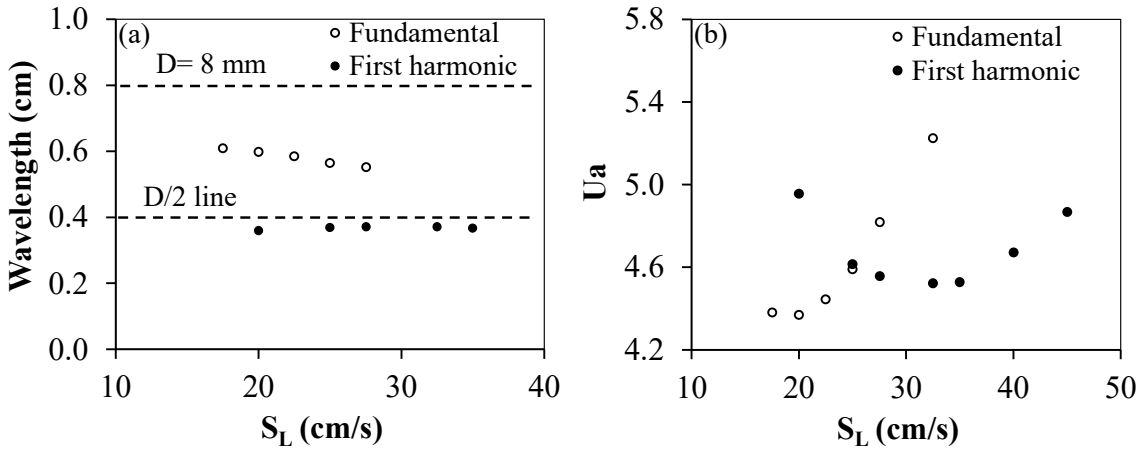

Fig. 21. Theoretical predictions showing a) effect of frequency on wavelength for *Le*=1.05 b) effect of frequency on critical acoustic velocity for *Le*=1.05 c) effect of *Le* at S_L=22.5 cm/s.

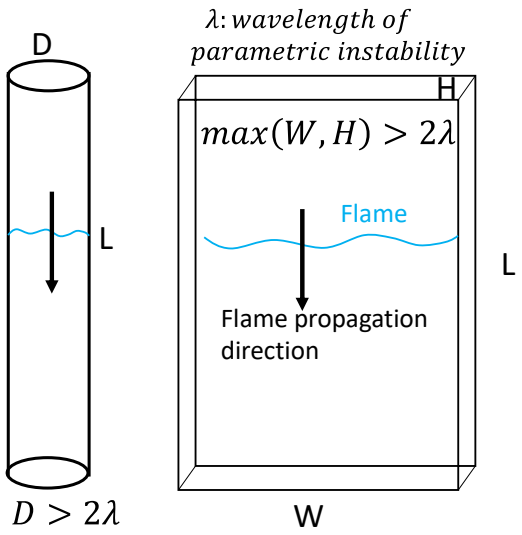

Fig. 22. Condition on geometry of tubes and Hele-Shaw cells for parametric instability

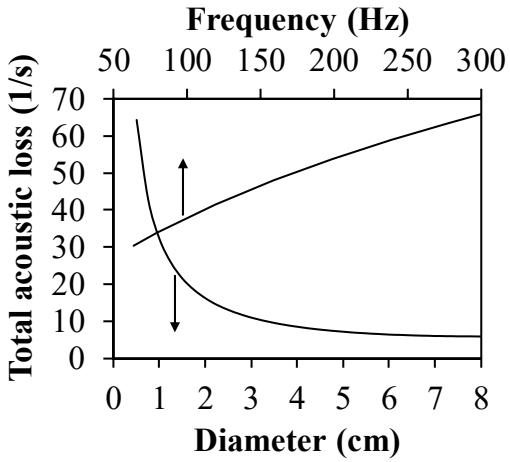

Fig. 23. Variation of acoustic losses with diameter of tube (at constant frequency of 110 Hz) and frequency (at constant diameter of 0.8 cm). The arrows indicate the direction in which horizontal axis of the curve should be seen.

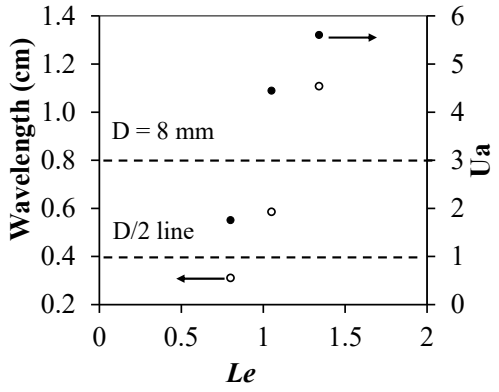

Fig. 24. Theoretical predictions showing effect of *Le* at S_L=22.5 cm/s wavelength and critical acoustic velocity of parametric instability of fundamental mode of tube (90 Hz).